Effects of spacer layers on magnetic properties and exchange couplings of Nd–Fe–B/Nd–Ce–Fe–B multilayer films*

Ya-Chao Sun(孙亚超)[1], Ming-Gang Zhu(朱明刚)[1,†], Wei Liu(刘伟)[2], Rui Han(韩瑞)[1], Wen-Chen Zhang(张文臣)[1], Yan-Feng Li(李岩峰)[1], and Wei Li(李卫)[1]

[1] *Division of Functional Materials, Central Iron & Steel Research Institute, Beijing* 100081, *China*

[2] *Shenyang National Laboratory for Materials Science, Institute of Metal Research, Chinese Academy of Sciences, Shenyang* 110016, *China*

(Received 15 May 2017; revised manuscript received 7 July 2017; published online 20 August 2017)

The influences of the spacer-layer Ta on the structures and magnetic properties of NdFeB/NdCeFeB multilayer films are investigated via DC sputtering under an Ar pressure of 1.2 Pa. An obvious (00l) texture of the hard phase is observed in each of the films, which indicates that the main phase of the film does not significantly change with Ta spacer-layer thickness. As a result, both the remanence and the saturation magnetization of the magnet first increase and then decrease, and the maximum values of $4\pi M_r$ and H_{cj} are 10.4 kGs (1 Gs = 10^{-4} T) and 15.0 kOe (1 Oe = 79.5775 A·m^{-1}) for the film with a 2-nm-thick Ta spacer-layer, respectively, where the crystalline structures are columnar shape particles. The measured relationship between irreversible portion $D(H) = -\Delta M_{irr}/2M_r$ and H indicates that the nucleation field of the film decreases with spacer layer thickness increasing, owing to slightly disordered grains near the interface between different magnetic layers.

Keywords: permanent magnets, multilayer films, spacer layer, irreversible

PACS: 75.70.–i, 75.60.Nt, 68.55.–a **DOI:** 10.1088/1674-1056/26/10/107501

1. Introduction

Due to the highest maximum energy product (BH)max among permanent magnets, Nd–Fe–B magnets have been widely used in different fields. In particular, the permanent magnets are used in auto industry such as motors for hybrid vehicles, electric vehicles and power steering. Hence the production and application of Nd–Fe–B magnets have been increased enormously.[1–3] To take full advantage of rich resources, the effort to reduce the amount of neodymium in Nd–Fe–B magnet by substituting partial Nd with cerium has been made in recent years. For economic and environmental pressures arising from the large-scale consumption of neodymium,[4–10] some work has been done to apply cerium to magnets. However, the crystal anisotropy field of 4.6 T of $Ce_2Fe_{14}B$ is only approximately half that of $Nd_2Fe_{14}B$ (7.5 T), the saturation magnetization of $Ce_2Fe_{14}B$ (1.17 T) is substantially lower than that of $Nd_2Fe_{14}B$ (1.61 T).[11] Thus, the substitution of cerium will lead to the decrease of remanence and intrinsic coercivity.

The intergrain and interlayer exchange coupling result from the nanometric structure, which has attracted much attention because of its influence on magnetism. Recently, we reported that the magnetic properties of sintered Nd–Ce–Fe–B magnet are not reduced as expected theoretically.[12,13] Somehow, the cerium effect in sintered magnet such as the multiple grain structure formed in magnet is complex. In this paper, we investigate the structures and magnetic properties of Nd–Ce–Fe–B film magnets, especially in the exchange coupling between the hard phases of the Nd–Ce–Fe–B multilayer films with textured structure. A Ta spacer layer serves as a way which can be effective for preventing interdiffusion in the interface region between the hard-magnetic layers in the multilayer film. In addition, the influences of the thickness of spacer layer on the structures and magnetic properties of the films are investigated.

2. Experimental procedure

Nanocomposites NdFeB(100 nm)/Ta(x)/(NdCe)FeB (100 nm)/Ta(x)/NdFeB(100 nm) (x = 0, 2, 5, 10, and 20 nm) multilayer films with Ta buffer layers and cover layers have been fabricated on Si substrates by DC sputtering. In this paper, a Ta buffer layer of 50 nm and a cover layer of 40 nm were sputtered at room temperature to align the easy axis of the $Nd_2Fe_{14}B$ grains, perpendicular to the film planes and to prevent the magnetic films from oxidizing. Also, the Ta spacer layers were deposited at room temperature with a speed of 1.5 nm/min. The Nd–Fe–B and (NdCe)–Fe–B magnetic layers were deposited at 903 K and proceeded with an in-situ rapid thermal annealing at 948 K for 30 min. The base pressure was better than 7.0×10^{-6} Pa, and the Ar pressure for sputtering was 1.2 Pa. The thickness values of the films were measured by weighing samples. The microstructures of phases in the films were identified by x-ray diffraction using Cu K_α

*Project supported by the Major State Basic Research Development Program of China (Grant No. 2014CB643701) and the General Program of the National Natural Science Foundation of China (Grant No. 51571064).

†Corresponding author. E-mail: mgzhu@sina.com

© 2017 Chinese Physical Society and IOP Publishing Ltd

radiation and transmission electron microscopy (TEM). The magnetic properties of the films were measured with a physical property measurement system (PPMS) and vibrating sample magnetometer (VSM). Moreover, all hysteresis loops are measured along the direction perpendicular to the thin film.

The Henkel curves have been used to study more details of the exchange coupling for multilayer film. The Henkel plot is as follows: $\delta_m(H) = [M_d(H) - M_r(\infty) + 2M_r(H)]/M_r(\infty)$, where $M_r(H)$ is acquired after the application and subsequent removal of a direct field H, $M_d(H)$ after dc saturation in one direction and the application and subsequent removal of a direct field H in the reverse direction, and $M_r(\infty)$ is the saturation remanence. According to the Wohlfarth's analysis,[14–16] the positive value of δ_m is due to the exchange coupling interaction, while the negative value of δ_m represents the dipolar interaction.

3. Results and discussion

Figure 1 shows the XRD patterns of Si/Ta/NdFeB(100 nm) /Ta(x)/(NdCe)FeB(100 nm)/Ta(x)/NdFeB(100 nm)/Ta ($x = 0$, 5, 20 nm) prepared by being deposited on the Si substrate at 903 K. The XRD patterns show that the magnetic main phase $(NdCe)_2Fe_{14}B$ coexists with Nd-rich phase, Si and Fe in the films. XRD peaks of the tetragonal $(NdCe)_2Fe_{14}B$ phase with an obvious (00l) texture are observed, which indicates that the main phase of the films does not significantly change with thickness of Ta spacer-layers. Similar XRD patterns are also obtained from all other films, indicating a c-axis textured structure is also realized in each of all films.

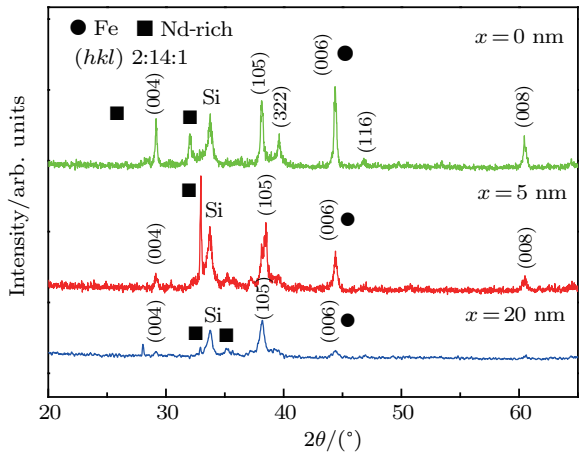


Fig. 1. (color online) XRD patterns of Si/Ta/NdFeB(100 nm)/Ta(x)/(NdCe) FeB(100 nm)/Ta(x)/NdFeB(100 nm)/Ta ($x = 0$, 5, 20 nm) thin films prepared by being deposited on the Si substrates at 903 K.

Figure 2 shows the out-of-plane hysteresis loops for Si/Ta/NdFeB(100 nm)/Ta(x)/(NdCe)FeB(100 nm)/Ta(x)/NdFeB(100 nm)/Ta ($x = 0$, 2, 5, 10, and 20 nm) films measured at room temperature. The permanent magnet performances, i.e., the values of M_r and H_{cj} are observed to be as high as $4\pi M_r$ = 10.4 kGs and H_{cj} = 15.0 kOe for the film with a 2-nm-thick Ta spacer-layer. It is clear that the hysteresis loops each with a good squareness are presented for the films with $x = 0$, 2 and 5 nm, indicating that the columnar grains grow along the direction perpendicular to the film plane, which is in agreement with results of XRD patterns and TEM observation. Moreover, kink is observed on none of the hysteresis loops of the films with $x = 0$, 2, and 5 nm, suggesting that the exchange coupling exists between the different hard magnetic layers. However, as for films with x = 10 nm and 20 nm, the magnetic properties decline rapidly, due to exchange decoupling effect.

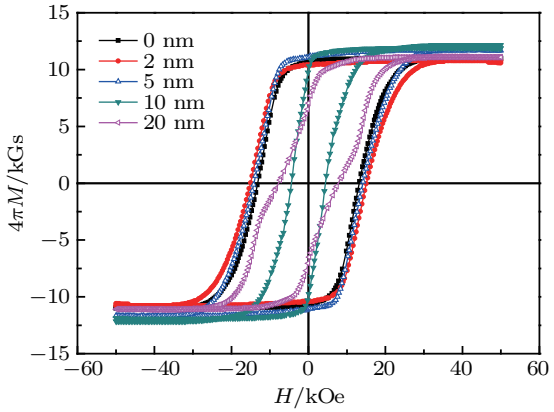


Fig. 2. (color online) Perpendicular hysteresis curves, observed at room temperature, for Si/Ta/NdFeB (100 nm)/Ta (x)/(NdCe)FeB(100 nm)/Ta(x)/NdFeB(100 nm)/Ta ($x = 0$, 2, 5, 10, and 20 nm) multilayer films deposited at 903 K with annealing at 948 K for 30 min.

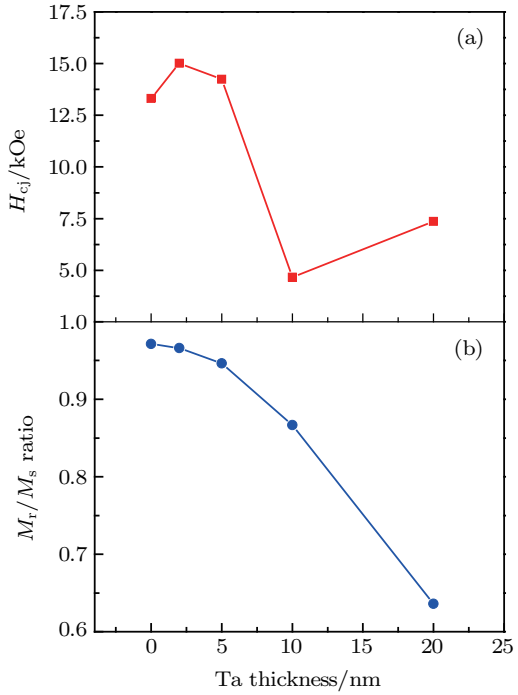


Fig. 3. (color online) Ta layer thickness-dependent H_{cj} (a) and M_r/M_s ratio (b) for Si/Ta/NdFeB (100 nm)/Ta(x)/(NdCe)FeB (100 nm)/Ta(x)/NdFeB(100 nm)/Ta ($x = 0$, 2, 5, 10, 20 nm) multilayer films deposited at 903 K and annealed at 948 K.

The Ta layer thickness-dependent coercivity and M_r/M_s ratio measured along the perpendicular direction are shown in Figs. 3(a) and 3(b). The coercivity of each of these films first

increases and then decreases with increasing x value, while the M_r/M_s ratio for each of the films decreases monotonically from 0.97 for $x = 0$ nm to 0.64 for $x = 20$ nm. The initial increase in the coercivity of the film with $x = 2$ nm is attributed to the enhancement of the exchange coupling between the different hard magnetic layers, which results from the addition of Ta spacer layer. The gradual decrease of the M_r/M_s ratio is due to the volume fraction of the hard magnetic phase decreasing.

Figures 4(a) and 4(b) show the transmission electron microscopy microstructures of Si/Ta/NdFeB(100 nm)/(NdCe)FeB(y)/NdFeB(100 nm)/Ta, with $y = 10$ nm and $y = 100$ nm, respectively. TEM observation shows that most of the crystalline grains are of columnar shape and obvious grain boundaries exist, which is in accordance with XRD results. Furthermore, there are many small disorder grains close to the buffer layer, which deteriorate the magnetic properties, and the thicker the spacer layer, the more the isolated small grains.

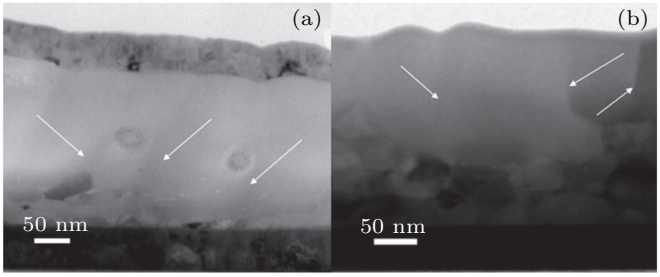


Fig. 4. The transmission electron microscopy images of the cross-section surface of the Si/Ta/NdFeB(100 nm)/(NdCe)FeB(y)/ NdFeB(100 nm)/Ta films, with (a) $y = 10$ nm and (b) $y = 100$ nm.

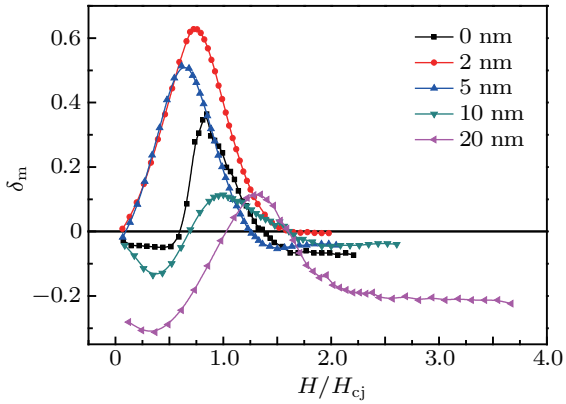


Fig. 5. (color online) The Henkel curves of Si/Ta/NdFeB (100 nm)/Ta(x)/(NdCe)FeB(100 nm)/Ta(x)/NdFeB(100 nm)/Ta ($x =$ 0, 2, 5, 10, and 20 nm) multilayer films.

The δ_m–H curves of Si/Ta/NdFeB(100 nm)/Ta(x)/(NdCe)FeB(100 nm)/Ta(x)/ NdFeB(100 nm)/Ta ($x = 0$, 2, 5, 10, 20 nm) multilayer films are shown in Fig. 5. It can be seen that the trilayer film with $x = 2$ nm possesses the higher positive peak value, which is in accordance with coercivity result. As the x value increases, the positive peak value for each of δ_m plots shows a "first increasing and then decreasing" tendency, which means that the thickness of spacer layer has an influence on exchange coupling interaction.

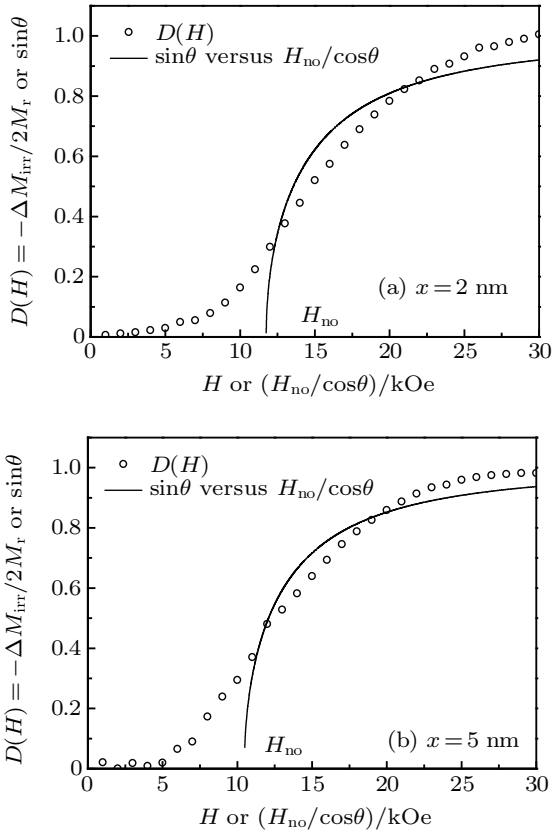


Fig. 6. Measured plots of irreversible portion $D(H) = -\Delta M_{irr}/2M_r$ versus H for Si/Ta/NdFeB(100 nm)/Ta(x)/(NdCe)FeB(100 nm)/Ta(x)/NdFeB(100 nm)/Ta films with (a) $x = 2$ nm and (b) $x = 5$ nm.

In order to further investigate the magnetic behaviors of the multilayer films depending on the spacer layer thickness, it is useful to analyze the irreversible portion in the dc demagnetization curve. The irreversible portion is described by the dc field demagnetization of the remanence $M_d(H)$, the remanence that is acquired after saturation in one direction and subsequent application of a dc field H in the opposite direction. Figure 6 shows the plot of the reduced irreversible portion as measured on the Si/Ta/NdFeB(100 nm)/Ta(x)/(NdCe)FeB(100 nm)/Ta(x)/NdFeB(100 nm)/Ta ($x = 2$ and 5 nm) films. No magnetization reversal occurs before the reverse field H increases the nucleation field H_{no}. When H increases further to a value $H_1 = H_{no}/\cos\theta_1$, for example, all regions with $0 \le \theta \le \theta_1$ reverse, where θ is the angle between reverse magnetic field and easy axis of grain. In that case, $H_n(\theta) = H_n(0)/\cos\theta = H_{no}/\cos\theta$, and the total irreversible change in magnetization is $2M_r\int_0^{\theta_1}\cos\theta\,d\theta = 2M_r\sin\theta_1$. The theoretical curve $\sin\theta$ versus $H_{no}/\cos\theta$ corresponds to the Kondorski model of completely inhomogeneous rotation.[14] Thus, the nucleation fields of 11.7 kOe and 10.5 kOe are obtained by fitting the experimental $D(H)$ data to the curve of $\sin\theta$ versus $H_{no}/\cos\theta$. The nucleation field of these films decreases with spacer layer thickness increasing. In fact, as the spacer layer thickness increases, more small grains which are unevenly distributed near the interface between different magnetic layers can be found.

Those disordered grains will affect angle θ, thereby influencing the nucleation field. Moreover, the nucleation fields of all those films are smaller than their coercivities.

4. Conclusions

The $Nd_2Fe_{14}B$-type hard-phase single layer films and nanocomposites $Nd_2Fe_{14}B/(NdCe)_2Fe_{14}B/Nd_2Fe_{14}B$ multilayer films are fabricated on the Si substrates with the different thickness Ta spacer layers by DC sputtering. The coercivity for each of these films first increases and then decreases with spacer layer thickness increasing, while the M_r/M_s ratio for each of the films decreases monotonically. The maximum values of $4\pi M_r$ and H_{cj} are 10.4 kGs and 15.0 kOe for the film with $x = 2$ nm. The results of δ_m plots suggest that there are strong exchange coupling interactions in the multilayer films. By improving the microstructure of the film, the disordered small grains near the buffer layer and spacer layers can be reduced, thereby increasing the nucleation field of film, to further improve the magnetic properties. The appropriately thick spacer layers are essential to the enhancement of exchange coupling interaction in multilayer film.

References

[1] Sagawa M, Togawa N, Yamamoto H and Matsuura Y 1984 *J. Appl. Phys.* **55** 2083
[2] Sato T, Oka N, Ohsuna T, Kaneko Y, Suzuki S and Shima T 2011 *J. Appl. Phys.* **110** 023903
[3] Wang W J, Guo Z H, Li A H, Li X M and Li W 2006 *J. Magn. Magn. Mater.* **303** 392
[4] Gong W and Hadjipanayis G C 1988 *J. Appl. Phys.* **63** 3513
[5] Yamasaki J, Soeda H, Yanagida M, Mohri K, Teshima N, Kohmoto O, Yoneyama T and Yamaguchi N 1986 *IEEE Trans. Magn.* **22** 763
[6] Ko K Y, Yoon S, Booth J G, Al-Kanani H J and Cho S K 2002 *J. Mater. Sci.* **37** 1421
[7] Ko K Y, Yoon S and Booth J G 1997 *J. Magn. Magn. Mater.* **176** 313
[8] Bulyk I I, Panasyuk V V, Trostianchyn A M, Grygorenko G M, Pomarin Y M, Taranova T G, Kostin V A and Putilov Y G 2004 *J. Alloys Compd.* **370** 261
[9] Niu E, Chen Z A, Chen G A, Zhao Y G, Zhang J, Rao X L, Hu B P and Wang Z X 2014 *J. Appl. Phys.* **115** 113912
[10] Huang S L, Feng H B, Zhu M G, Li A H, Sun Y C, Zhang Y and Li W 2015 *J. Miner. Metall. Mater.* **22** 417
[11] Herbst J F 1991 *Rev. Mod. Phys.* **63** 819
[12] Huang S L, Feng H B, Zhu M G, Li A H, Zhang Y and Li W 2014 *AIP Adv.* **4** 107127
[13] Zhu M G, Li W, Wang J D, Zheng L Y, Li Y F, Zhang K, Feng H B and Liu T 2014 *IEEE Trans. Magn.* **50** 1000104
[14] Kneller E F and Hawig R 1991 *IEEE Trans. Magn.* **27** 3588
[15] Zhang H W, Rong C B, Du X B, Zhang J, Zhang S Y and Shen B G 2003 *Appl. Phys. Lett.* **82** 4098
[16] Kelly P E, Grady K O, Mayo P I and Chantrell R W 1989 *IEEE Trans. Magn.* **25** 3881